biophysica

MDPI

Article

DNA and RNA Helices as Antennae for Sonic and Electromagnetic Communication

Allan Widom [1,†], John Swain [1], Yogendra Srivastava [1,*], Georges de Montmollin [2], David Drosdoff [3], Meenakshi Narain [4,†] and Elisabetta Sassaroli [5]

[1] Physics Department, Northeastern University, Boston, MA 02115, USA
[2] Lenr-Cities Suisse Sárl, Rue Charles-Knapp 29, CH-2000 Neuchâtel, Switzerland; georges@montmollin.ch
[3] Physical Sciences Department, Tulsa Community College, Tulsa, OK 74115, USA; david.drosdoff@tulsacc.edu
[4] Physics Department, Brown University, Providence, RI 02912, USA
[5] Physics Department, MassBay Community College, Wellesley, MA 02481, USA; elisabetta.sassaroli@gmail.com
* Correspondence: yogendra.srivastava@gmail.com
† Deceased.

Abstract

In addition to the electrogenic microorganisms, e.g., bacteria, that can be found in communities that are wired together in circuits carrying electrons in and out of biological cells, strong evidence exists that there are wireless connections between micro-organisms that pass information to one another at a distance in virtue of electromagnetic signals. One needs electromagnetic antennae to send or receive signals as they pass information back and forth between living microorganisms. We here discuss the properties of DNA and RNA long polymer molecules regarding their utility as antennae. As well as emitting or absorbing radiation photons, these antennae also emit and absorb phonons, i.e., acoustic signals. The coupling between sound waves and electromagnetic waves is very appreciable and is described by biological piezoelectricity. Biological phases of condensed matter also exhibit chiral symmetry breaking, i.e., "handedness" symmetry breaking, between right- and left-handed electronic states. Describing two spin components (say up and down) times two chirality components (say left and right) ultimately requires four-component electron wave functions as discovered by Dirac even if the electrons are moving at velocities much less than light speed. Coupled with the quasi-one-dimensional nature of long polymer molecules, this yields bound Bose-condensed particle-hole pairs constituting a Tomonaga–Luttinger liquid similar in some ways to the Bardeen–Cooper–Schriefer Bose-condensed bound electron pairs found in superconductors. One similarity is that transport weak links in the Bose condensate fluid flow yield Josephson effects described by a quantum pendulum, e.g., a sine-Gordon field theory. The coherent phase in the Tomonaga–Luttinger liquid is the difference between the right- and left-handed electronic phases, as first demonstrated by Coleman via the conversion of the massive Thirring model into a Josephson-type pendulum model. The complete theory of wireless communication between biological organisms is only beginning to be developed. The basic DNA and RNA microbe antennae must be wired in nature as a coherent phased antenna array for appreciable communication bit rates radiated through large distances. Finally, acoustic and/or radio frequency electromagnetic radiation carrying sufficient communication information should be of use medically as a possible alternative to chemical medicines and/or vaccines in the treatment of illness; for a most recent example in the COVID-19 virus with its RNA internal antenna.

Check for updates

Academic Editor: Shin-ichi Tate

Received: 16 August 2026
Revised: 22 September 2026
Accepted: 25 September 2026
Published: 29 September 2026

Copyright: © 2026 by the authors. Licensee MDPI, Basel, Switzerland. This article is an open access article distributed under the terms and conditions of the Creative Commons Attribution (CC BY) license.

Keywords: sonic and electromagnetic communication; bacteria; theory

1. Introduction

There is a substantial literature describing the long-wavelength excitations of long-chain organic polymer biomolecules by quantum field theories in one spatial dimension (See, for example [1,2]). The applications of quantum field theoretic statistical thermodynamics [3] to the biological mantra that proteins are fabricated and controlled by mathematical computational programs contained within DNA and RNA macro-molecules [4] have thus far still been limited. Ultimately, the methods of quantum field theory should be applicable to medicinal practice such as the development of alternatives to standard vaccines applied to the maladies of some DNA molecules within bacteria and some RNA molecules within viruses. Our purpose is to provide some initial stages towards studying field theoretical models. Applications to the avatars of RNA of the COVID-19 virus would have some immediate importance.

The microscopic theory of condensed matter physics that can be used for understanding forces in biological matter must be based on the quantum electrodynamic interaction in continuous media [5]. At the classical level, the Lagrangian method employed for describing photons and collective electromagnetic field configurations is fairly well known [5] (Sec. 62). Field quantization follows the canonical rules. For weak excitations in long chain biomolecules, the effective Lagrangians describe bosons computed by functionally integrating out Fermion electron interactions. Purely electron charge transport can then be described by boson fields of the effective Lagrangian employing topologically charged soliton excitations. The mathematical properties of such soliton solutions of the boson equations of motion are very well established [6]. In what follows, we consider electronic charge transport along DNA and RNA long-chain molecules responsible for inducing electromagnetic antenna processes wherein low-frequency radio and acoustic-frequency phonons and photons [7–10] can be emitted and absorbed [5] (Sec. 91).

For the case of bacteria, there exist electronic communications within large communities because, within a single community, different cells are biologically wired to one another and circuit electrons pass through the biological mesh wiring through cell walls. A single bacterium with one or more connection wires allowing electrons to pass across the cell wall is often called an electrogenic bacterium. Studies of electrogenic bacterial communities abound [11–14] and engineering applications are beginning. For example, one may produce chemical batteries with electromotive forces induced by bacteria [15]. However, the electricity in this case is maintained by wiring some bacteria to other bacteria and/or by wiring bacteria to chemical cell electrode surfaces.

Shewanella oneidensis MR-1 cells are rod-shaped bacteria measuring [2–3 μm] in length and [0.4–0.7] μm in diameter. Their nanowires or outer membrane extensions (often called bacterial appendages) have a diameter between [3–5 nm] for thin single filaments; between [90–150 nm] for pilus-like bundled structures and their isolated tubular extensions have lateral diameters about 100 nm and height ranging between [5–10 nm]. Their length can range from tens of microns to several micrometers. The scale can be approximately estimated through the resolution of SEM [0.5–4 nm] and the number of long and thick appendages visible in part (a) of Figure 1.

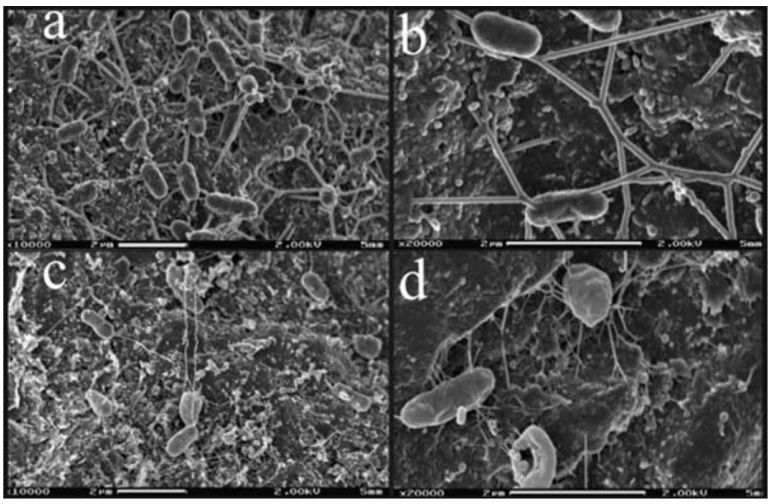

Figure 1. SEM images. (**a**) Pilus-like appendages from *S. oneidensis* MR-1. Appendages are long and thick. (**b**) Close-up image showing a network of cell-cell and cell-mineral connections, merging and splitting of appendages. (**c**,**d**) Pilus-like appendages from *S. oneidensis* mutant strain showing thin and frail appendages and cells are visibly deteriorated. For details, see text. Reproduced from [16] with permission from John Wiley and Sons.

In Section 2, we present different perspectives within which the problem of information in biological systems has been approached and investigated by researchers.

Of central interest in this work is the wireless electrodynamic connections between bacteria and/or viruses.

2. Methods: Information in Biology and DNA/Biomaterial EM Waves

In a seminal paper, Crick laid down the *central dogma* of molecular biology [17]:

> *the transfer of information from nucleic acid to nucleic acid, or from nucleic acid to protein may be possible, but transfer from protein to protein, or from protein to nucleic acid is impossible. Information means here the precise determination of sequence, either of bases in the nucleic acid or of amino acid residues in the protein.*

Thus, genetic information flows only one way: from DNA to RNA to proteins. Among other things, it justified a central notion in biology that acquired characteristics cannot be inherited [18,19]. However, as chronicled by Artiga [20], instead of curtailing the debate on the issue of genes carrying information, it opened the floodgates on what information and communication are; on the role of evolution in biological information; upon whether Shannon [21] or decisional concepts are or should be the guiding elements about information in biology. See, for example: [22–27]. As very clearly stated by Koonin [23]:

> *Biological information encoded in genomes is fundamentally different from and effectively orthogonal to Shannon entropy. The biologically relevant concept of information has to do with 'meaning', i.e., encoding various biological functions with various degrees of evolutionary conservation.*

Lest there be any misunderstanding about what the present paper is about, let us state that as physicists our goal is quite modest and limited in scope to deriving results that are (at least in principle) experimentally testable. As in our first paper on the subject [10], we continue to employ Shannon's connection between entropy and information and augmented by the second law of thermodynamics, we were able to prove a theorem about the minimum energy dissipated into the environment in any classical computation.

Equation (2.6) in [10] states that the minimum dissipated energy (ΔE) for a program using (ΔN) bits of memory is given by

$$\Delta E \geq (k_B T)(ln2)\Delta N \tag{1}$$

As most of the present paper deals with quantum aspects of biology, combined with the general belief that (for human beings) a four-letter genetic program of a few gigabytes is stored on each DNA molecule, it is worthwhile to quote the following from [10]:

> *This constitutes an irreversible thermodynamic second law bound on the heat of a classical computation. In principle, a quantum computation can be made reversible but only at the expense of leaving quantum bits of information in a superposition of different states. On the other hand, a memory bit in a quantum superposition of states is unreadable. It is a very basic Bohr principle of quantum mechanics that all measurable data are classical. Thus, Equation (1) is expected to hold true for all computations with output (readable) data.*

We applied thermodynamic reasoning using the above concepts of information and entropy to a DNA molecule. The normal coiled state of the DNA molecule can become uncoiled. It is experimentally possible to hold two points of a long molecule apart with optical tweezers and measure the molecular tension (τ).

As shown in our reference [10], if ($\mathcal{L}$) denotes the distance between the two points, then thermodynamics relates the DNA molecular free energy (F) at temperature (T) to variations in the tension (τ) and length ($\mathcal{L}$):

$$dF = -\mathcal{S}dT + \tau d\mathcal{L} = -(k_b ln2)NdT + \tau d\mathcal{L};$$

$$\text{Thus, information per unit length :}$$

$$\left(\frac{\partial N}{\partial \mathcal{L}}\right)_T = -\left(\frac{1}{k_b ln2}\right)\left(\frac{\partial \tau}{\partial T}\right)_L. \tag{2}$$

From known variations of tension with temperature, we were able to estimate for DNA molecules an information density of 30 gigabytes per meter, comparable to the total information stored in DNA. This is an important result not only in its own right because it is correct but also because it confirms the relevance of the Shannon theory to the information content of a DNA molecule. We are unaware of any other formalism leading to a similar estimate from first principles.

We next tackled the problem of *memory* of water in which most DNA is located. One property that goes far in establishing water to be quintessential for life is that water contains ordered electric dipoles of radius ($R \approx 100$ nm), due to a condensation of photons interacting with molecular dipole moments [28,29]. The ordered domains in water [30,31] yield an anomalously high water heat of vaporization (q^*/molecule $\approx$ 0.53 eV).

Let (Δs) and (Δv) be the gain in entropy and the volume of a single molecule as it evaporates from the liquid into the vapor. The information per molecule may then be measured through the vapor pressure co-existence curve:

$$\left(\frac{dP}{dT}\right) = \frac{\Delta s}{\Delta v} = \frac{q^*}{T\Delta v} = \frac{(k_B ln2)N^*}{\Delta v} \tag{3}$$

The anomalously high value of the heat of vaporization (q^*/molecule) noted above leads to a high degree of memory storage capacity $N^* = 23.5$ bits/water molecule.

Similarly, the partial entropy per molecule of an ion species dissolved in an aqueous electrolyte [32,33] has a sufficiently high bit of information per ion for it to get attached to an ordered domain of water. This increase in the bulk coherent ordering volume of quantum hydration captured by an ion allows for semi-permeable membranes which can either pass

an ion through a small gap or forbid such passage depending in part on the state of order in the ion attachment. Such passage through or rejection from semi-permeable membranes based on information (or equivalently entropy) constitutes a program for biological cells closely analogous to polymer DNA-based programs. The ionic flow through membranes in nerve cells allows for human memory storage in nerve cell networks residing in the human brain. Thus, as noted in [10], these have about the same order of magnitude of biological information capacity density, which far surpasses information density stored in commercial computer memory devices.

We now turn to a discussion of expected wave patterns in biology through the example of what we call the DNA waves. As stressed in our paper [8], photosynthesis, whose source is a long-distant Sun, provides a simple counterexample to the widely held view that biochemistry encompasses only short-range molecular rearrangement interactions. Thus, as biochemical reactions can be induced at a distance due to the propagation of electromagnetic (EM) signals at optical frequencies, we investigated EM signals from biological materials at much lower frequencies and found the following results:

A. Low Frequency Noise: In the regime of very low frequencies, [1 Hz $< (\omega/2\pi) <$ 20 Hz], spectral noise can appear from the electronic magnetic moment precession due to small magnetic fields. Even if the shielding of magnetic fields due to external sources were perfect, the thermal fluctuations of coil currents would still give rise to magnetic fields yielding low-frequency noise signals. The value of thermal magnetic fields (B_T) from thermal fluctuations in a cylindrical vessel carrying water of volume (V) at temperature (T) was estimated and employed using the equipartition theorem to estimate the frequency (f_T) produced both for orbital and spin parts using the gyromagnetic ratio (γ) for electronic currents [Equation (13) reference [8]]:

$$\begin{aligned} B_T &= \sqrt{\frac{4\pi k_B T}{V}}; \\ 2\pi f_T = |\gamma| B_T;\ \gamma &= \frac{e}{2mc} = -\frac{(8.79 \times 10^6)}{Gauss\ s.}; \\ f_T^{orbital} &= (1.01\ Hz)\sqrt{\left(\frac{cm^3}{V}\right)\left(\frac{T}{300\ K}\right)}; \\ f_T^{spin} &= (2.02\ Hz)\sqrt{\left(\frac{cm^3}{V}\right)\left(\frac{T}{300\ K}\right)}; \end{aligned} \tag{4}$$

Experimental evidence for a signal at ($f \approx 7$ Hz) for diluted bacterial DNA samples in water obtained by the Montagnier group [34] is in agreement with our estimate. The magnetic field value in Equation (4) is internal to the system and will hold true only if external magnetic fields are sufficiently well screened.

B. High Frequency Noise: We modeled an electron that can move around a bacterial DNA loop of effective length (L), including the windings of helices and along the ordered water layers within which the DNA is stored. A reasonable Hamiltonian model for the electronic energy levels was chosen as

$$\begin{aligned} H &= \frac{1}{2m}\left(-i\hbar\frac{d}{ds} - \frac{e}{c}A(s)\right)^2 + V(s); \\ V(s) &= V(s+L);\ A(s) = A(s+L); \end{aligned} \tag{5}$$

wherein the allowed electronic wave function has the periodicity $\psi(s) = \psi(s + L)$ around the DNA loop. Similarly, the vector potential $A(s)$ tangential to the DNA loop can be expanded generically as follows, respecting the strict periodicity

$$A(s) = \frac{\Phi}{L} + \sum_{n}^{\infty} A_n \, cos\Big(\frac{2\pi n s}{L} + \vartheta_n\Big) \tag{6}$$

With an intelligent choice of a gauge function [*vedi* Equation (17) of reference [8]], the above Hamiltonian can be simplified to

$$\begin{aligned} H_{eff} &= \frac{1}{2m}\Big(-i\hbar\frac{d}{ds} - \frac{e\Phi}{cL}\Big)^2 + V(s); \\ \psi(s) &= \psi(s + L);\ V(s) = V(s + L). \end{aligned} \tag{7}$$

For a successful comparison with experimental data [34] on K-12 E. Coli with a total putative length $\hat{L} \approx 0.157$ cm, we had to assume that the electron can skip rungs of a DNA around ordered water, thereby shortening the length to half its value, $L \approx 0.086$ cm. Then, for zero magnetic flux and a uniform potential, we derived

$$\Delta f = \frac{2\pi\hbar}{mL^2} \approx\ 1\ KHZ; \tag{8}$$

in good agreement with the experimental data. Considering the complexity of the problem and the simplicity of the model, the results are more than satisfactory.

In a recent precision experiment [35] (see also [36]), EM signals from biofilms were carefully recorded for a long period and the results were carefully analyzed. We quote from [35]

> *This paper reports the first successful detection of electromagnetic (EM) radiation from Staphylococcus aureus biofilms in the gigahertz (GHz) frequency range. Two novel sensing systems are deployed for the measurement. A very sensitive wide-band near-zone radiative system specifically designed for this application is first used to search for signals in the 1–50 GHz frequency region. Notable radiation is observed in the 3–4 GHz band. Exposure to lethal doses of Zinc oxide nano-pyramids (ZnO-NPY) is used to verify that the signals are indeed produced by living cells rather than material thermal emission. Afterward, a spiral antenna system is exploited to further examine the band of interest in the near-field region. Radiation from three identical biofilm samples is monitored and recorded over 70 days. Two distinct frequency bands, namely the 3.18 GHz and the 3.45 GHz bands, are identified as potential "communication bands". Furthermore, long-term and short-term cycles of the total radiation intensity within the band are observed over the course of the experiment. This work confirms the presence of EM radiation within bacterial communities, which is a key requirement to demonstrate EM signaling among bacterial cells. The insight could lead to breakthroughs in demystifying how cells communicate as well as advancement of important technologies in biology and communication systems.*

Indeed, these results should alleviate some doubt as to the veracity of EM signals arising from living systems and thus communications therefrom. And as more research is conducted on the subject matter, further experimental data will emerge to corroborate or dispute these notions. In Appendix A, we shall present some medical applications of sonic and EM signals that have been experimentally tested.

3. Results

3.1. EM Radiations from One-Dimensional Sources

In wireless connections, information is emitted or detected in antennae that can radiate and absorb electromagnetic radiation from a distance. In particular, our purpose is to further elaborate on the antenna emission and absorption properties of long DNA and RNA molecules. In fact, work has already started on wireless bacterial/virus communication, both experimentally [34] and theoretically, quantum mechanically [7,8,10] through the RNA and DNA molecules and more recently from a more classical perspective via amyloid fibrils [36]. Since these long polymer molecules are quasi-one-dimensional, the electrical currents that emit or absorb radiation photons may be adequately described by one-dimensional quantum electrodynamic models, and these shall be essential to our general approach. In addition to photon excitations in the DNA and RNA molecules, there exist bosonic mechanical phonon oscillations, i.e., acoustic vibrations. The phonon-photon interaction thereby describes a piezoelectric effect in DNA and RNA molecules that occurs due to the chiral or handedness symmetry breaking of the helical molecules that are double-stranded for DNA and single-stranded for RNA. The symmetry breaking must thereby be included in the one spatial dimensional field theoretical models employed to describe biological piezoelectricity [37,38]. Ultimately, this requires Dirac electron matrices that have dimension four, i.e., two spin states times two chiral states. Employing one spatial dimensional Dirac spinors, these four states can be handled as two states in computational time.

The notion of describing electron charged currents in one spatial dimensional models with boson fields is very well known and constitutes the physical basis of Tomonaga–Luttinger fermion liquid models [1,39–41]. A central physical point is that a locally conserved charge in a model in one space plus one time dimension obeys the local charge conservation law $\partial_\mu J^\mu = 0$. In field theories with one spatial dimension

$$\frac{\partial \lambda(z,t)}{\partial t} + \frac{\partial I(z,t)}{\partial z} = 0, \tag{9}$$

wherein $\lambda(z,t)$ and $I(z,t)$ represent, respectively, the charge density per unit length and the current. For the problem of wireless communication between different DNA or RNA long polymer helical molecules, Equation (9) represents the antenna current along the molecule emitting and absorbing radiation. The general solution to the local charge conservation Equation (9) involves the dipole moment per unit length $Q(z,t)$ defined to obey

$$I(z,t) = \frac{\partial Q(z,t)}{\partial t} \quad \text{and} \quad \lambda(z,t) = -\frac{\partial Q(z,t)}{\partial z}. \tag{10}$$

Thus, the electrical currents in one-plus-one-dimensional field theories can be described by a single scalar boson field $Q(z,t)$ having physical dimension of charge regardless of the fermion field dynamics that may be at the root of the physical motions.

3.1.1. Cable Photons in DNA and RNA Chains

Short-ranged heavy massive boson exchange can lead in the vacuum to a point-like Fermion interaction between currents. boson masses in biological matter are here considered massive if $M_{(\text{heavy boson})}c^2/e \gg 1$ millivolt. The semiconducting electrons in electrodynamic coherent water [42] domains set the voltage scale of millivolts for the electronic semiconducting energy gaps in biology. For quantum field theories in one spatial dimension, the photons can travel along the molecules as E waves or TM cable modes or as B waves or TE cable modes. TE and TM modes along one-dimensional cables are massive and exchange of such photons in one spatial dimension leads to the Fermi electronic point-

like or at least short-ranged interaction. The vacuum interaction depends on the square of the current $J_\mu J^\mu = I^2 - c^2\lambda^2$.

Since the long DNA or RNA chains reside in solution, there is a capacitance per unit chain length ε and an inductance per unit chain length μ. In Appendix A, we show graphs for the expected capacitance and inductance per unit length for chains in water with variable salinity.

The condensed matter Fermi current-current interaction is a simple TEM massless photon. In Gaussian electromagnetic units, there is a zero-mass TEM cable-mode Lagrangian as grown out of the biological matter point-like Fermi interaction in one spatial dimension

$$\begin{aligned} L_{TEM} &= \frac{1}{2}\int_{\mathcal{L}}\left[\mu I^2 - \frac{1}{\varepsilon}\lambda^2\right]dz, \\ L_{TEM} &= \frac{1}{2}\int_{\mathcal{L}}\left[\mu\left(\frac{\partial Q}{\partial t}\right)^2 - \frac{1}{\varepsilon}\left(\frac{\partial Q}{\partial z}\right)^2\right]dz, \\ v &= \frac{1}{\sqrt{\mu\varepsilon}} \quad \text{wherein} \quad v = \text{TEM photon velocity.} \end{aligned} \tag{11}$$

The quantum electrodynamic zero-mass photon quantization from the Lagrangian Equation (11) is canonical and describes the Goldstone boson for the ordered Tomonaga–Luttinger liquid of electrons.

3.1.2. Polymer Chain Thermodynamics

In Section 3.2 the statistical thermodynamics of a long polymer molecule having energy $\mathcal{U}$, entropy $\mathcal{S}$, length $\mathcal{L}$, dipole moment $\mathcal{P}$ and chemical composition particle numbers $\mathcal{N}_1, \ldots, \mathcal{N}_f$ will be discussed in terms of the complete extensive scaling thermodynamic function

$$\begin{aligned} &\mathcal{U} = \mathcal{U}(\mathcal{S}, \mathcal{L}, \mathcal{P}, \mathcal{N}_1, \ldots, \mathcal{N}_f), \\ &\lambda\mathcal{U} = \mathcal{U}(\lambda\mathcal{S}, \lambda\mathcal{L}, \lambda\mathcal{P}, \lambda\mathcal{N}_1, \ldots, \lambda\mathcal{N}_f), \\ &d\mathcal{U} = Td\mathcal{S} + \tau d\mathcal{L} + Ed\mathcal{P} + \sum_{a=1}^{f}\mu_a d\mathcal{N}_a, \\ &\mathcal{U} = T\mathcal{S} + \tau\mathcal{L} + E\mathcal{P} + \sum_{a=1}^{f}\mu_a\mathcal{N}_a, \end{aligned} \tag{12}$$

wherein T, τ, E, and $\mu_1 \ldots, \mu_f$ represent, respectively, the temperature, long molecule tension (negative compression), electric field tangent to the molecule axis and chemical potentials. In terms of intensive quantities per unit length

$$\begin{aligned} &\mathcal{U} = u\mathcal{L}, \quad \mathcal{S} = s\mathcal{L}, \quad \mathcal{P} = Q\mathcal{L}, \quad \mathcal{N}_a = \Gamma_a\mathcal{L}, \\ &u = Ts + \tau + EQ + \sum_{a=1}^{f}\mu_a\Gamma_a, \\ &-d\tau = sdT + QdE + \sum_{a=1}^{f}\Gamma_a d\mu_a, \\ &du = Tds + EdQ + \sum_{a=1}^{f}\mu_a d\Gamma_a. \end{aligned} \tag{13}$$

The complete thermodynamic intensive energy per unit length function $u(s, Q, \Gamma_1, \ldots, \Gamma_f) \equiv u(s, Q, \Gamma)$ determines the dipole moment per unit length function $Q(s, E, \Gamma)$,

$$Q = -\left(\frac{\partial \tau}{\partial E}\right)_{T,\boldsymbol{\mu}} = -\left(\frac{\partial w}{\partial E}\right)_{s,\boldsymbol{\Gamma}}$$
$$w(s, E, \Gamma) = \inf_{Q}(u(s, Q, \boldsymbol{\Gamma}) - EQ)$$
$$dw = Tds - QdE + \sum_{a=1}^{f} \mu_a d\Gamma_a. \tag{14}$$

The thermodynamic equations of state may be computed from field theoretical models in one spatial z plus one temporal t dimension wherein the spatial coordinate z represents the distance along the axis of the molecule. The current Equations (9) and (10) along the molecular axis is completely determined by Q obeying in thermodynamics Equation (14). Finally, the full Lagrangian for molecular polymer antennae currents reads

$$L_{electronic}[Q] = \int_{\mathcal{L}} \left\{ \frac{1}{2\varepsilon} \left[\frac{1}{v^2} \left(\frac{\partial Q}{\partial t} \right)^2 - \left(\frac{\partial Q}{\partial z} \right)^2 \right] - u(s, Q, \boldsymbol{\Gamma}) \right\} dz. \tag{15}$$

The quantum electrodynamic antenna photon quantization from the Lagrangian Equation (15) is canonical. Equation (15) holds true in virtue of Equations (11) and (13). The above Lagrangian, Equation (15), is a central result of this work on DNA and RNA antennae.

Ordinary Helmholtz linear electric dipole antennae or loop magnetic dipole antennae are designed employing the physics of linear electromagnetic equations in matter as in the Lagrangian Equation (11). Nature's biological antennae design has been more inventive than Helmholtz's, employing nonlinear effects and yielding electronic currents for emitting and absorbing photons described by soliton transport. Previously, this approach has proved successful in describing polyacetylene and magnetic dipole rings of $(CH)_n$ of the benzene ring (n = 6) type.

Finally, additional dissipation processes increasing entropy (s) in the antennae will give rise to finite lifetime effects for the non-linear collective photon solitons. However, these lifetimes become limited to large times by the semiconductor soliton topological stability, which amounts to identifying soliton fundamental homotopy group kinks as physical electronic charges. Some discussion of photon and phonon absorption is given in Section 3.4.

3.1.3. Field Theoretical Models

The simplest example of the field theoretical models applied to a long organic polymer molecule involved trans-polyacetylene, whose chain of n links has the chemical formula $(CH)_n$ and is pictured in Figure 2. The $(CH)_n$ polymer chain, though different from RNA/DNA molecules, may serve as a powerful analogy for the main discussion. Indeed, one key notion is that certain facts are manifested from the 1-dimensional topology and features, instead of the exact chemical composition.

The fermion electronic model in one spatial dimension involves the massive Thirring model with a Dirac spinor band kinetic energy plus the Fermi pointwise current–current electron interaction. This point-like Fermi interaction can be renormalized only in a one spatial dimension field theory. Such a Fermion model can also be "bosonized" as noted by Tomonaga [39], Luttinger [40] and Mattis and Lieb [41]. A relativistic view of the renormalized massive Thirring model in one spatial dimension was discussed in great mathematical detail by Coleman [43] who proved the "bosonized" equivalence to the sine-Gordon field theory in one spatial dimension. The connection between the soliton

in the quantum field theoretical sine-Gordon model and electronic charge transport in polyacetylene polymer chains was discussed in the work on the SSH model [44,45] (Su, Schrieffer, Heeger).

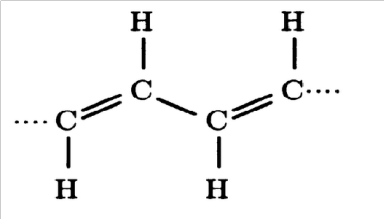

Figure 2. Shown is the molecular structure of a polyacetylene chain (CH)n of n links. Each carbon atom bonds to a neighboring carbon atom, alternating between one and two bonds as in $\cdots - C = C - C = C - C = C - \ldots$. The fourth carbon bond is attached to a hydrogen atom. A chain of six links completed as a hexagon represents C6H6 = (CH)6, i.e., a benzene ring. A chain completed into a ring or loop acts as a molecular magnetic dipole antenna. Such would also be true of a polymer DNA loop in bacteria or an RNA loop in a virus.

The nature of the soliton Fermion number was explored by Jackiw and Rebbi [46]. In our work, the soliton has the charge of one electronic charge as demanded by the connection between local charge conservation and gauge invariance. The soliton structure has been reported and observed [47]. The Coleman sine-Gordon equivalence is discussed in Section 3.3.

3.1.4. The Mechanics of Damped Slinky Modes

The two-helix DNA model and the single-helix RNA model mechanically act similarly to a quantum mechanical molecular toy helical slinky. The known mechanical modes of motion of such a slinky are usually called wormlike in conventional studies [48] of long polymer chains. The statistical mechanics [49] of the slinky or wormlike motions wherein the long helical biological molecules clump into balls of string or are knitted and folded into sheets of polymer protein material is well studied. These have long been applied to describe biological compaction essential for the central biological mantra of how DNA and RNA produce proteins. These compaction modes are discussed in Section 3.4.

The differential geometry of the path of a long spatial winding polymer chain is described by giving the points on a polymer path [50] as a function of arclength s,

$$\mathbf{r} = \mathbf{r}(s) \quad \text{wherein} \quad ds^2 = d\mathbf{r} \cdot d\mathbf{r}. \tag{16}$$

A triad of unit vectors, one tangent $\mathbf{t}$ and two normal $\mathbf{n}$ and $\mathbf{b} = \mathbf{t} \times \mathbf{n}$, creates a moving reference frame triad of unit vectors $(\mathbf{t}, \mathbf{n}, \mathbf{b})$ along the curved molecular path. The rotation of the unit orthonormal vector triad obeys.

The equations of Frenet and Serret,

$$\frac{d}{ds}\begin{pmatrix}\mathbf{t}\\ \mathbf{n}\\ \mathbf{b}\end{pmatrix} = \begin{pmatrix}0 & \kappa & 0\\ -\kappa & 0 & \tilde{\tau}\\ 0 & -\tilde{\tau} & 0\end{pmatrix}\begin{pmatrix}\mathbf{t}\\ \mathbf{n}\\ \mathbf{b}\end{pmatrix}, \tag{17}$$

wherein κ is the curvature of the molecule and $\tilde{\tau}$ is the torsion of the molecule. In order to understand the meaning of curvature and torsion, consider the case wherein the curvature and torsion are uniform along the curve, i.e.,

$$\kappa = \frac{R}{R^2 + [h/(2\pi)]^2}, \quad \tilde{\tau} = \frac{[h/(2\pi)]}{R^2 + [h/(2\pi)]^2} \tag{18}$$

for the case that R = const. and h = const. generates a helix as shown in Figure 3.

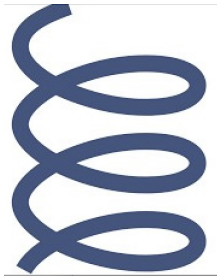

Figure 3. Shown is the helix of radius R and pitch h generated by constant curvature and constant torsion as in Equation (18) below. R is the radius of the helical cylinder, and for every 2π rotation around the cylinder axis the curve rises a height h.

In the Kratky–Porod model, also known as the wormlike chain model [48,51,52], the DNA and/or RNA polymer helices wiggle about like worms in the fluid solute environment. The energy of a worm-like chain or, more briefly, a deformed slinky-wormlike polymer is described by the energy

$$\mathcal{U}_{deformation} = \tau\mathcal{L} + \frac{\mathcal{Y}}{2}\int_{\mathcal{L}}\left[\xi_1^4\kappa(s)^2 + \xi_2^4(\tilde{\tau}(s) - \tilde{\tau}_0)^2\right]ds, \tag{19}$$

wherein for tension, $\tau > 0$, or compression, $\tau < 0$. This first term treats the wormlike slinky motions as in string theory with the long chain molecular "string" embedded in the physical three spatial dimensions. The second two terms on the right-hand side of Equation (19) give rise to rigidity in transverse mechanical vibrations and in torsional (or angular) mechanical vibrations that affect the mechanical vibrations, giving rigidity to the polymer chain. The Young's modulus is denoted by $\mathcal{Y}$ and the Poisson ratio is denoted by σ. Finally, the persistence lengths of the polymer rigidity will be denoted by ξ_j. Here we are applying classical elasticity theory [53]. In bulk solids, there is one longitudinal sound wave velocity and two modes of transverse sound velocity as given by

$$\begin{aligned} v_{long} &= \sqrt{\frac{\mathcal{Y}(1-\sigma)}{\rho(1-\sigma)(1-2\sigma)}} \quad \text{Bulk Longitudinal} \\ v_{trans} &= \sqrt{\frac{\mathcal{Y}}{2\rho(1+\sigma)}} \quad \text{Bulk Transverse.} \end{aligned} \tag{20}$$

Finally, the persistence lengths of the polymer rigidity will be denoted by ξ_j.

There are four modes of mechanical waves on helical polymer molecules in a worm-like chain as shown in Figure 4. There exist four kinds of mechanical waves of interest: (i) There are two longitudinal modes with a straight line z-axis as the center of the coils. There is compressional sound in a cylinder, and rotational sound due to torsion. (ii) There are two transverse degrees of freedom for the now curved central axis of the coil as in Equation (19).

Associated with bulk polymer mass density ρ is a longitudinal persistence length ξ_l defined thermodynamically by

$$\rho_1 \equiv \left(\sum_{a=1}^{f} m_a\Gamma_a\right) = \rho\xi_l^2, \tag{21}$$

wherein m_a is the mass of chemical species a on the polymer chain, and ρ_1 is the mass per unit length of the chain.

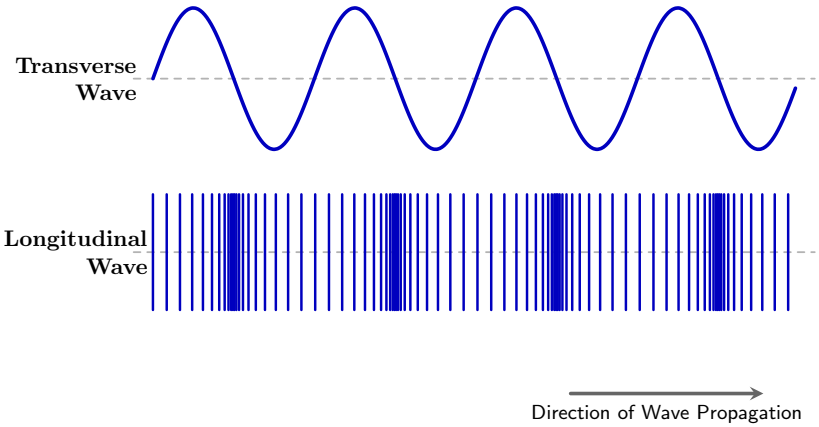

Figure 4. Shown schematically above are two longitudinal modes and two transverse modes. The longitudinal modes are determined if the "center line" of the helices is straight. The two longitudinal degrees of freedom can be taken as R(z,t), the local radius of the straight coil, and h(z,t), the local pitch of the straight coil. The z-axis is a straight line. The physical picture of the two longitudinal modes is linear compression and local rotational displacement, both with an associated Poisson ratio. The two transverse modes have curved central lines with arc length ds and distortion energy given by Equation (19).

For small oscillations in the elastic strain, the first longitudinal compressional mode in a thin straight worm slinky has a sound velocity spectrum

$$\omega = v_l k \quad \text{compressional} \quad v_l = \sqrt{\frac{\mathcal{Y}}{\rho}}. \tag{22}$$

The second straight central axis mode is torsional, with spectrum

$$\omega = D_l k^2 \quad \text{torsional} \quad D_l = v_l \xi_l. \tag{23}$$

Typically, longitudinal compressional mode velocities $v_l \sim 2 \times 10^5$ cm/s, while persistence lengths are approximately the coherent domain sizes in water [42,54], $\xi \sim 5 \times 10^{-6}$ cm. Thus, $D_l \sim 1$ cm^2/s. Note the electron quantum of circulation $D_{el} = (\hbar/m) \approx 1.16$ cm^2/s contributing to the free electron spectrum $E = \hbar^2 k^2/(2m)$. The agreement $D_{el} \sim D_l$ is not fortuitous. Finally, the transverse bending modes for the wormlike-slinky have the spectrum

$$\omega = D_t k^2 \quad \text{transverse} \quad D_l = v_t \xi_t, \tag{24}$$

which is degenerate if the straight-line axis does not sense an asymmetry in the rotational moments of inertia. Here ξ_t is the transverse persistence length. These frequencies, quadratic in the wave number k, are comparable to free electron Bohr transition frequencies, $\hbar\omega_{fi} = E_f - E_i$, wherein $E = \hbar^2 k^2/(2m)$ and obey

$$\omega_{fi} = \frac{1}{2} D_{el} \Big[(k_f + k_i)(k_f - k_i) \Big] \quad \text{with} \quad D_{el} = \frac{\hbar}{m}. \tag{25}$$

The similar orders of magnitude $D_l \sim D_{el}$ are not fortuitous. Young's modulus describes the internal pressure-energy as determined by the electron Pauli exclusion principle required for stable matter when Coulomb forces are of microscopic importance.

3.1.5. Electric and Magnetic Dipole Antennae

In Section 3.3, the electric dipole antenna that constitutes a linear axis DNA or RNA chain polymer molecule subject to an electric field is described by the massive Thirring sine Gordon Lagrangian in a driving electric E field

$$L_{electronic}[Q] = \left(\frac{1}{2\varepsilon}\right) \times \int_{\mathcal{L}} \left[\frac{1}{v^2}\left(\frac{\partial Q}{\partial t}\right)^2 - \left(\frac{\partial Q}{\partial z}\right)^2\right] dz - \int_{\mathcal{L}} \left[\hbar\overline{\omega}\left(1 - \cos\left(2\pi\frac{Q}{e}\right)\right) - EQ\right] dz, \tag{26}$$

corresponding to the equation of motion

$$\frac{1}{\varepsilon}\left[\frac{1}{v^2}\left(\frac{\partial}{\partial t}\right)^2 - \left(\frac{\partial}{\partial z}\right)^2\right] Q + \left(\frac{2\pi\hbar\overline{\omega}}{e}\right) \sin\left(2\pi\frac{Q}{e}\right) = E. \tag{27}$$

If the driving electric field depends only on time,

$$E(t) = -\frac{1}{c}\dot{A}(t) \quad \text{and} \quad \mathcal{P} = \mathcal{L}Q(t), \tag{28}$$

then only the total electric dipole moment $\mathcal{P}$ comes into the equations of motion. In the electric dipole limit, we thereby have the ordinary differential equation corresponding to a voltage $V(t)$ driven pendulum with a current output $I(t) = \dot{Q}(t)$,

$$L\ddot{Q}(t) + V_c \sin\left(2\pi\frac{Q(t)}{e}\right) = V(t), \tag{29}$$

wherein the antenna inductance $L = \mu\mathcal{L}$, the driving voltage $V(t) = E(t)\mathcal{L}$ and the critical voltage is defined $V_c = (2\pi\hbar\overline{\omega}/e)\mathcal{L}$. If the electron oscillations on the straight axis of the antenna have a finite dissipation, increasing the molecular entropy by heating, then phenomenologically a resistance R may be added to the electric dipole antenna model according to $I(t) = \dot{Q}(t)$,

$$L\ddot{Q}(t) + R\dot{Q}(t) + V_c \sin\left(2\pi\frac{Q(t)}{e}\right) = V(t). \tag{30}$$

For the moment, neglecting resistance, the driven electric dipole antenna acts as a quantum electrodynamic circuit described by the ordinary Lagrangian

$$\Lambda(\dot{Q}, Q) = \frac{L}{2}\dot{Q}^2 + \frac{\mathcal{L}A\dot{Q}}{c} - \left(\frac{eV_c}{2\pi}\right)\left[1 - \cos\left(2\pi\frac{Q}{e}\right)\right] \tag{31}$$

in virtue of Equation (29). The Hamiltonian operator corresponding to the Lagrangian Equation (31) is canonical,

$$\mathcal{H}(\Phi_{ext}) = \frac{1}{2L}\left(-i\hbar\frac{\partial}{\partial Q} - \frac{\Phi_{ext}}{c}\right)^2 + \left(\frac{eV_c}{2\pi}\right)\left[1 - \cos\left(2\pi\frac{Q}{e}\right)\right]. \tag{32}$$

Here the driving vector potential is $A = \Phi_{ext}/\mathcal{L}$. By wrapping up the linear electric dipole antenna into a loop, one obtains the magnetic dipole antenna with a total magnetic moment given by a current-area product.

In detail, the external magnetic flux through the loop is given by

$$\Phi_{ext} = \oint \mathbf{A} \cdot d\mathbf{r} = \int_{\mathcal{L}} Ads. \tag{33}$$

The Schrödinger equation for the loop is given by

$$i\hbar\frac{\partial\phi(Q,t)}{\partial t} = \mathcal{H}(\Phi_{ext})\phi(Q,t), \tag{34}$$

wherein the Hamiltonian is identical to the electric dipole antenna Hamiltonian in Equation (32). However, the magnetic dipole antenna boundary condition defining the geometrical meaning of "loop" is the magnetic dipole boundary periodic condition

$$\phi(Q+e,t) = \phi(Q,t) \quad \text{magnetic dipole loop.} \tag{35}$$

In particular, as a consequence of Equation (35), the energy eigenvalues are periodic in external magnetic flux, i.e.,

$$\begin{aligned} \mathcal{H}(\Phi_{ext})\phi_n(Q) &= E_n(\Phi_{ext})\phi_n(Q), \\ \phi_n(Q+e) &= \phi_n(Q), \\ E_n(\Phi_{ext}+\Phi_0) &= E_n(\Phi_{ext}), \end{aligned} \tag{36}$$

wherein the flux quantum is given by

$$\Phi_0 = \frac{2\pi\hbar c}{e}. \tag{37}$$

According to present international agreements on SI units, where the electromagnetic charge conversion is exactly 1 emu ≡10 Coulomb and 1 Tesla ≡10^4 Gauss, we have the exact three-unit definitions

$$\begin{aligned} c &\equiv 2.99792458 \times 10^{10}\ \text{cm/s}, \\ 2\pi\hbar &\equiv 6.62607015 \times 10^{-27}\ \text{erg s}, \\ \frac{e}{c} &\equiv 1.602176634 \times 10^{-20}\ \text{emu}. \end{aligned} \tag{38}$$

The flux quantum is then

$$\Phi_0 \approx 4.135667697 \times 10^{-7}\ \text{Gauss cm}^2. \tag{39}$$

Many distinctive properties of DNA or RNA molecular antennae follow from the periodicities of the circulating currents

$$I_n(\Phi_{ext}) = I_n(\Phi_{ext} + \Phi_0). \tag{40}$$

Equation (40) follows from

$$I_n(\Phi_{ext}) = -c\frac{dE_n(\Phi_{ext})}{d\Phi_{ext}} \tag{41}$$

in virtue of Equation (37). The magnetic flux periodicity of circulating currents in molecular dipole antennae arises out of electrodynamic gauge invariance and the Bohm–Aharonov effect and is likely to surpass the accuracy of a particular model Hamiltonian such as ours and play a strong role in wireless transmission of information between DNA and/or RNA molecules.

3.2. Statistical Thermodynamics

Of interest here are electrical and mechanical vibrations that quantize into photons and phonons in the usual manner. Photon-phonon conversions can and do take the form of piezoelectricity that goes into the design of ultrasound emitters and absorbers [55]. A simple understanding of piezoelectricity can be obtained by the general principles of statistical thermodynamics. The role of this reasoning is of use for understanding biological piezoelectricity as it occurs in long strands of DNA and RNA due to the lack of chiral (handed) symmetry in helical molecules.

3.2.1. Quartz Crystal Ultrasound

To obtain ultrasound generators from a quartz crystal, it is sufficient to cleave the crystal so that a given crystal plane appears parallel on two sides of the quartz sample. Then deposit two metallic films, one on each of the opposite flat sides of the quartz sample, forming a circuit capacitor and add equal and opposite charges on the two metallic plates. The thermodynamic equations of state of the capacitor follow from the fundamental law

$$d\mathcal{U} = Td\mathcal{S} + \mathcal{V}dQ + \mathcal{F}dX, \tag{42}$$

wherein $\mathcal{S}$, Q and X represent, respectively, the capacitor entropy, charge and quartz crystal plane displacement and T, $\mathcal{V}$, and $\mathcal{F}$ represent, respectively, the capacitor temperature, voltage and force component parallel to the plane displacement that the metallic film exerts on the quartz crystal. Alternatively, one may employ the capacitor enthalpy

$$\begin{aligned} \mathcal{W}(\mathcal{S}, \mathcal{V}, X) &= \min_{Q}[\mathcal{U}(\mathcal{S}, Q, X) - \mathcal{V}Q], \\ dW &= Td\mathcal{S} - Qd\mathcal{V} + \mathcal{F}dX. \end{aligned} \tag{43}$$

The capacitances at constant displacement X and at constant force $\mathcal{F}$ are defined, respectively, as

$$C_X = \left(\frac{\partial Q}{\partial V}\right)_{\mathcal{S},X} \quad \text{and} \quad C_{\mathcal{F}} = \left(\frac{\partial Q}{\partial \mathcal{V}}\right)_{\mathcal{S},\mathcal{F}}. \tag{44}$$

Employing the thermodynamic derivative identities

$$\left(\frac{\partial Q}{\partial \mathcal{V}}\right)_{\mathcal{S},\mathcal{F}} = \left(\frac{\partial Q}{\partial \mathcal{V}}\right)_{\mathcal{S},X} + \left(\frac{\partial Q}{\partial X}\right)_{\mathcal{S},\mathcal{V}}\left(\frac{\partial X}{\partial \mathcal{V}}\right)_{\mathcal{S},\mathcal{F}},$$
$$C_{\mathcal{F}} = C_X - \left(\frac{\partial Q}{\partial X}\right)_{\mathcal{S},\mathcal{V}}\left(\frac{\partial X}{\partial \mathcal{F}}\right)_{\mathcal{S},\mathcal{V}}\left(\frac{\partial \mathcal{F}}{\partial \mathcal{V}}\right)_{\mathcal{S},X},$$
$$C_{\mathcal{F}} = C_X + \frac{\Lambda_{\mathcal{S}}^2}{K_{\mathcal{S}}}, \tag{45}$$

wherein the adiabatic piezoelectric coefficient is defined by a Maxwell relation for the enthalpy Equation (43)

$$\Lambda_{\mathcal{S}} = \left(\frac{\partial Q}{\partial X}\right)_{\mathcal{S},\mathcal{V}} = -\left(\frac{\partial \mathcal{F}}{\partial \mathcal{V}}\right)_{\mathcal{S},X}. \tag{46}$$

The thermodynamic adiabatic static Hooke's law spring constant for the vibrational quartz mode is defined as

$$\mathcal{K}_{\mathcal{S}} = \left(\frac{\partial \mathcal{F}}{\partial X}\right)_{\mathcal{S},\mathcal{V}}. \tag{47}$$

The central result of this section is that a measured capacitance of the quartz-filled capacitor is a circuit parallel connection between two capacitors: (i) a capacitance C_X wherein the position of the vibrational mode is clamped and (ii) an elastic capacitance

$$C_{\mathcal{F}} = C_X + C_{\text{elastic}},$$
$$C_{\text{elastic}} = \frac{\Lambda_{\mathcal{S}}^2}{\mathcal{K}_{\mathcal{S}}}, \tag{48}$$

adding capacitance for the parallel circuit connection. Using a damped harmonic oscillator model for the quartz vibrational phonon mode yields a complex frequency-dependent elastic electrical engineering capacitance

$$\mathcal{M}\delta\ddot{X}(t) + \mathcal{R}\delta\dot{X}(t) + \mathcal{K}_{\mathcal{S}}\delta X(t) = \delta\mathcal{F}(t),$$
$$C_{\text{elastic}}(\omega) = \frac{\Lambda_{\mathcal{S}}^2}{\mathcal{K}_{\mathcal{S}} - i\omega\mathcal{R} - \omega^2\mathcal{M}},$$
$$C_{\text{elastic}}(\omega) = \frac{\omega_0^2 C_{\text{elastic}}}{\omega_0^2 - i\Gamma\omega - \omega^2}. \tag{49}$$

wherein $\mathcal{M}$ is the mass of the vibrational mode and $\mathcal{R}$ is the mechanical acoustic impedance of the vibrational mode. The frequency ω_0 of the quartz phonon mode and the inverse phonon lifetime $\tau_{phonon}^{-1} = \Gamma$ are determined in mechanical engineering terms by

$$\omega_0 = \sqrt{\frac{\mathcal{K}_{\mathcal{S}}}{\mathcal{M}}} \quad \text{and} \quad \Gamma = \frac{\mathcal{R}}{\mathcal{M}}. \tag{50}$$

The frequency-dependent circuit admittance of the fixed displacement capacitance connected in parallel with the elastic mode capacitance is

$$Y(\omega) = -i\omega[C_X + C_{\text{elastic}}(\omega)],$$
$$Y(\omega) = -i\omega\left[C_X + \frac{\omega_0^2 C_{\text{elastic}}}{\omega_0^2 - i\Gamma\omega - \omega^2}\right],$$
$$\Re e Y(\omega) = \omega_0^2\Gamma\left[\frac{\omega}{(\omega^2 - \omega_0^2)^2 + \omega^2\Gamma^2}\right]C_{\text{elastic}}. \tag{51}$$

If a voltage source $\mathcal{V}_\omega$ at frequency ω is placed across the quartz crystal-filled capacitor, then the dissipated power $P(\omega) = |\mathcal{V}_\omega|^2 \Re e Y(\omega)$ is mostly due to a sharp phonon peak as described by Equation (51). The dissipative power mostly goes into phonon radiation from the quartz mechanical oscillator that becomes a source of ultrasound at a sharp frequency. Let us now apply similar thermodynamic arguments to long DNA and RNA molecules as we have above reviewed for standard ultrasonic crystal sources.

3.2.2. DNA and RNA Piezoelectricity

To describe the piezoelectric effect in DNA and RNA molecules, start from the dipole moment enthalpy

$$\begin{aligned}
&\tilde{\mathcal{W}} = \min_{\mathrm{Q}} \Big[\mathcal{U}(S, \mathcal{L}, \mathcal{P}, \mathcal{N}_1, \ldots, \mathcal{N}_f) - E\mathcal{P} \Big], \\
&\tilde{\mathcal{W}} = \tilde{\mathcal{W}}(S, \mathcal{L}, E, \mathcal{N}_1, \ldots, \mathcal{N}_f), \\
&d\tilde{\mathcal{W}} = Td\mathcal{S} + \tau d\mathcal{L} - \mathcal{P}dE + \sum_{a=1}^{f} \mu_a d\mathcal{N}_a, \\
&\tilde{\mathcal{W}} = T\mathcal{S} + \tau\mathcal{L} + \sum_{a=1}^{f} \mu_a \mathcal{N}_a.
\end{aligned} \tag{52}$$

With $\mathcal{N} = \sum_{a=1}^{f} \mathcal{N}_a$. The intensive per-constituent particles are defined as

$$\begin{aligned}
&x_a = \frac{\mathcal{N}_a}{\mathcal{N}}, \quad \sum_{a=1}^{f} x_a = 1, \\
&\tilde{w} = \frac{\tilde{\mathcal{W}}}{\mathcal{N}}, \quad \tilde{s} = \frac{\tilde{\mathcal{S}}}{\mathcal{N}}, \quad l = \frac{\tilde{\mathcal{L}}}{\mathcal{N}}, \quad \tilde{p} = \frac{\tilde{\mathcal{P}}}{\mathcal{N}} = lQ, \\
&\tilde{w} = T\tilde{s} + \tau l + \sum_{a=1}^{f} \mu_a x_a,
\end{aligned} \tag{53}$$

in view of which

$$d\tilde{w} = Td\tilde{s} + \tau dl - \tilde{p}dE + \sum_{a=1}^{f} \mu_a dx_a. \tag{54}$$

Static Piezoelectricity:

The static adiabatic piezoelectric coefficient of a long polymer molecule is defined as

$$\lambda_{\tilde{s}} = \left(\frac{\partial \tau}{\partial E} \right)_{\tilde{s},l,\mathbf{x}} = -\left(\frac{\partial \tilde{p}}{\partial l} \right)_{\tilde{s},E,\mathbf{x}}, \tag{55}$$

wherein a Maxwell relation implicit in Equation (54) has been employed. Two molecular polarizability coefficients may be defined (i) at constant molecular tension τ and (ii) at constant molecular length l; They are, respectively,

$$\alpha_\tau = \left(\frac{\partial \tilde{p}}{\partial E} \right)_{\tilde{s},\tau,\mathbf{x}} \quad \text{and} \quad \alpha_l = \left(\frac{\partial \tilde{p}}{\partial E} \right)_{\tilde{s},l,\mathbf{x}}. \tag{56}$$

The difference in partial differentials is evidently

$$\alpha_\tau = \alpha_l + \left(\frac{\partial \tilde{p}}{\partial l}\right)_{\tilde{s},l,\mathbf{x}} \left(\frac{\partial l}{\partial E}\right)_{\tilde{s},\tau,\mathbf{x}},$$
$$\alpha_\tau = \alpha_l - \left(\frac{\partial \tilde{p}}{\partial l}\right)_{\tilde{s},l,\mathbf{x}} \left(\frac{\partial l}{\partial \tau}\right)_{\tilde{s},E,\mathbf{x}} \left(\frac{\partial \tau}{\partial E}\right)_{\tilde{s},l,\mathbf{x}},$$
$$\alpha_\tau = \alpha_l + \frac{\lambda_{\tilde{s}}^2}{\kappa_{\tilde{s}}}, \tag{57}$$

wherein the Hooke law adiabatic spring constant $\kappa_{\tilde{s}}$ per molecule for a long molecule is defined by

$$\kappa_{\tilde{s}} = \left(\frac{\partial \tau}{\partial l}\right)_{\tilde{s},E,\mathbf{x}}. \tag{58}$$

The fundamental thermodynamics for piezoelectricity in long DNA or RNA molecular polarizability,

$$\alpha_\tau = \alpha_l + \alpha_{\text{elastic}} \quad \text{wherein} \quad \alpha_{\text{elastic}} = \frac{\lambda_{\tilde{s}}^2}{\kappa_{\tilde{s}}}, \tag{59}$$

plays the same role in long polymer piezoelectric physics that Equation (48) plays for quartz piezoelectricity.

Classical thermal fluctuations in the molecular tension obey

$$\overline{\Delta\tau^2} = \frac{k_B T}{\mathcal{N}} \left(\frac{\partial \tau}{\partial l}\right)_{\tilde{s},E,\mathbf{x}} = k_B T \left(\frac{\kappa_{\tilde{s}}}{\mathcal{N}}\right),$$
$$\overline{\Delta\tau^2} = k_B T \left(\frac{\partial \tau}{\partial \mathcal{L}}\right)_{\mathcal{S},E,\mathcal{N}_1,\ldots,\mathcal{N}_f} = k_B T \mathcal{K}_{\mathcal{S}}, \tag{60}$$

wherein the overall adiabatic spring constant of the molecule is inversely proportional to the number of constituent molecules $\mathcal{K}_{\mathcal{S}} = \kappa_{\tilde{s}}/\mathcal{N}$. On the other hand, the mode mass for a homogeneous slinky-worm oscillation is extensive, $\mathcal{M} = \mathcal{N} m_0$, where m_0 is the order of the mean molecular mass. This means that the frequency of the homogeneous compression mode is given by

$$\Omega = \sqrt{\frac{\mathcal{K}_{\mathcal{S}}}{\mathcal{M}}} = \frac{\omega_0}{\mathcal{N}} \to 0 \quad \text{as} \quad \mathcal{N} \to \infty. \tag{61}$$

Given the virtually zero frequency of the homogeneous longitudinal dissipation, the mode is completely dissipative.

The piezoelectric charge coefficient [d_{33}] quantifies the volume change in a piezoelectric material when impressed upon by an electric field or, otherwise said, the polarization generated under a given stress. This coefficient fluctuates between a fraction of pico-Coulomb/Newton and about 10 pico-Coulomb/Newton depending upon a variety of factors: ionic ambiance; levels of hydration and their means of measurement. As far as we are aware, no direct evaluation of acousto-electromagnetic conversion efficiency for nucleic acids has been reported in the published literature.

Vibrational Dissipation:

For mechanical vibrations coupling into antenna currents via piezoelectric coefficients, an engineering approach may generalize the static quartz oscillator coupling Equation (48) that in dynamic situations reads as Equation (49). The close analogy is that the dynamic engineering version of Equation (59) is given by

$$\alpha_\tau = \alpha_l + \alpha_{\text{elastic}} \sum_j \left[\frac{f_j \omega_j^2}{\omega_j^2 - i\Gamma_j - \omega^2}\right], \tag{62}$$

wherein the sum is over mechanical modes described by damped harmonic oscillators with oscillator strengths $f_j > 0$ that sum to unity, i.e., $\sum_j f_j = 1$. In Equation (62), ω_j represents the mechanical resonance frequency of the phonon and Γ_j represents the transition rate per unit time that the phonon is absorbed as heat energy into other degrees of freedom. One may introduce a damping force correlation time τ_j of the random force from these other degrees of freedom that damp the mechanical oscillation according to Fermi's golden rule

$$\Gamma_j = \frac{2\pi}{\hbar}|\hbar\omega_j|^2\left(\frac{\tau_j}{2\pi\hbar}\right),$$
$$\Gamma_j = \omega_j^2\tau_j \Rightarrow \frac{\Gamma_j}{\omega_j} = \omega_j\tau_j. \tag{63}$$

Equation (62) describes how the mechanical modes enter into the electrodynamic properties of DNA and RNA antennae only if the modes are lightly damped, $\omega_j\tau_j \ll 1$. If the phonon modes are very highly damped by viscous forces, then Equation (62) is not adequate. The physical principles follow below.

Consider the original Stokes problem, i.e., damping from a solid surface in contact with a viscous fluid. Consider the formally infinite surface problem wherein the solid is in the half-space $z < 0$, the viscous fluid is in the half-space $z > 0$, and the oscillation of the solid surface is in the x-direction. If $v_x(z,t)$ is the only non-zero fluid velocity component in the fluid mechanical Navier–Stokes equations, then the velocity $V(t)$ and the force per unit area that the fluid exerts on the solid surface $F(t)$ obey, respectively,

$$V(t) = \lim_{z\to 0^+} v_x(z,t) \quad \text{and}$$
$$F(t) = -\eta \lim_{z\to 0^+}\left(\frac{\partial v_x(z,t)}{\partial z}\right). \tag{64}$$

The velocity diffusion equation with viscosity η and mass density ρ is here written within the fluid as

$$\rho\frac{\partial v_x(z,t)}{\partial t} = \eta\frac{\partial^2 v_x(z,t)}{\partial z^2}. \tag{65}$$

In virtue of the fractional derivative identities [56] one may take the "operator square root" of Equation (65)

$$\sqrt{\rho\frac{\partial}{\partial t}}\,v_x(z,t) = \sqrt{\eta}\frac{\partial v_x(z,t)}{\partial z}, \tag{66}$$

yielding the force per unit area as a functional of the sliding surface velocity,

$$F(t) = -\sqrt{\rho\eta}\left[\sqrt{\frac{\partial}{\partial t}}\right]V(t),$$
$$F(t) = -\sqrt{\rho\eta}\left[\sqrt{\frac{1}{\pi}}\int_0^\infty \frac{ds}{\sqrt{s}}e^{-s\partial/\partial t}\right]V(t),$$
$$\frac{F(t)}{\rho} = -\sqrt{\frac{\nu}{\pi}}\int_0^\infty \frac{ds}{\sqrt{s}}V(t-s), \tag{67}$$

wherein $\eta = \rho\nu$ in virtue of Equation (64) and the evaluation of the integral $\sqrt{\pi a} = \int_0^\infty e^{-as}ds/\sqrt{s}$.

The drag force per unit surface area $[F(t)]$ is a nonlocal in time functional of the surface velocity $V(t)$ for an incompressible fluid with kinematic viscosity ν. The kinematic viscosity represents the diffusion of liquid vorticity at a rate in water of

$$\nu \approx 10^{-2}\,\frac{\mathrm{cm}^2}{\mathrm{s}} = 10^4\ \mathrm{Hz} \times (10\ \mathrm{micron})^2 \quad (\mathrm{water}). \tag{68}$$

For a distance ∼10 micron, say within a biological cell, for many types of cells, the mechanical modes exhibit strongly viscous damping for frequencies $\omega < 10$ kHz. The strong damping leads to a fractional exponent in the imaginary part of the dielectric response $\sim\omega^{-1/2}$ as $\omega \to 0$. Confinement geometries more generally lead to dynamic fractional exponents $\sim\omega^{-z}$ as $\omega \to 0$, even in pure water wherein the extremely high dielectric response as $\omega \to 0$ has a domain size scale of ordered water [42,54].

3.3. Massive QED Thirring Model

The mass term employing Dirac spinors yields the invariant energy density

$$u_{\mathrm{mass}} = -m_{\mathrm{electron}}c^2\bar{\psi}\psi, \tag{69}$$

wherein ψ is the electron wave function. If the Dirac matrices are written in the representation in which the left and right chiral matrices are diagonal, then the notion of mass comes from matrix elements that connect right to left chirality. In one spatial dimension, fix the spin and consider the two-element electron wave function for left- and right-handed electrons,

$$\psi = \begin{pmatrix} \psi_R \\ \psi_L \end{pmatrix} \quad \text{where} \quad \bar{\psi}\psi = \psi_R^*\psi_L + \psi_L^*\psi_R. \tag{70}$$

If the left and right amplitudes have phases,

$$\begin{aligned} \psi_{R,L} &= |\psi_{R,L}|e^{i\theta_{L,R}} \equiv \sqrt{\frac{n_{\mathrm{pair}}}{2}}e^{i\theta_{L,R}}, \\ \psi_R^*\psi_L + \psi_L^*\psi_R &= n_{\mathrm{pair}}\cos(\theta_R - \theta_L), \end{aligned} \tag{71}$$

where $n_{\mathrm{pair}} = (1/2)|\psi_R\psi_L|$ denotes the number of bound particle-hole pairs per unit length. Then the phase difference implicit in Equation (70)

$$\theta_R - \theta_L = 2\pi\frac{Q}{e}, \tag{72}$$

yields the energy density

$$u_{\mathrm{mass}} = -\hbar\overline{\omega}\cos\left(2\pi\frac{Q}{e}\right) \tag{73}$$

in virtue of quantum phase interference between the left- and right-handed chirality states. In Equation (73), $m_{\mathrm{electron}}c^2 n_{\mathrm{pair}} = \hbar\overline{\omega}$. A convention adds a constant to this energy to make a model energy density $u(Q)$,

$$u(Q) = \hbar\overline{\omega}\left[1 - \cos\left(2\pi\frac{Q}{e}\right)\right], \tag{74}$$

to employ in the Coleman sine Gordon Lagrangian Equation (26). This completes our derivation of Coleman's result that a massive Thirring Fermion model of electrons in a quasi-linear system is equivalent to a sine-Gordon boson model.

3.4. Slinky Damped Mechanics of the Longitudinal Sound Mode

Here we consider the viscous damping of a pure longitudinal wave in a slinky helix. The viscous damping is mainly due to the electronic viscosity that is, in turn, caused by the electrical conductivity. The molecular ultrasonic phonon absorption is thereby due to the electronic Landau–Fermi liquid conductivity in a bulk metal [55] (Chapter 12) but here is due to the Tomonoga–Luttinger [39–41] liquid in DNA or RNA long helical slinky polymer molecules. Thermodynamics, as dictated by Section **??**, is determined by

$$\begin{aligned} d\tilde{u} &= Td\tilde{s} + Ed\tilde{p} + \sum_{a=1}^{f} \mu_a dx_a, \\ d\tilde{w} &= Td\tilde{s} + \tau dl - \tilde{p}dE + \sum_{a=1}^{f} \mu_a dx_a, \end{aligned} \tag{75}$$

yielding the thermodynamic identity

$$\begin{aligned} \kappa_{\tilde{s}} &= \left(\frac{\partial \tau}{\partial l}\right)_{\tilde{s},E,\boldsymbol{x}}, \\ \kappa_{\tilde{s}} &= \left(\frac{\partial \tau}{\partial l}\right)_{\tilde{s},\tilde{p},\boldsymbol{x}} + \left(\frac{\partial \tilde{p}}{\partial l}\right)_{\tilde{s},E,\boldsymbol{x}} \left(\frac{\partial \tau}{\partial \tilde{p}}\right)_{\tilde{s},l,\boldsymbol{x}}, \\ \kappa_{\tilde{s}} &= \kappa_{\tilde{s}l} + \left(\frac{\partial \tilde{p}}{\partial l}\right)_{\tilde{s},E,\boldsymbol{x}} \left(\frac{\partial \tau}{\partial E}\right)_{\tilde{s},l,\boldsymbol{x}} \left(\frac{\partial E}{\partial \tilde{p}}\right)_{\tilde{s},l,\boldsymbol{x}}, \\ \kappa_{\tilde{s}} &= \kappa_{\tilde{s}l} - \left(\frac{\partial \tau}{\partial E}\right)^2_{\tilde{s},l,\boldsymbol{x}} \left(\frac{\partial E}{\partial \tilde{p}}\right)_{\tilde{s},l,\boldsymbol{x}}, \\ \kappa_{\tilde{s}} &= \kappa_{\tilde{s}l} - \left(\frac{\lambda_{\tilde{s}}^2}{\alpha_l}\right). \end{aligned} \tag{76}$$

To obtain the frequency-dependent Hooke's law force constant for a uniform compression or extension in electrical engineering terms, one extends Equation (76) to the upper half complex frequency plane $\zeta = \omega + i\overline{\omega}$ wherein $\overline{\omega} > 0$,

$$\kappa(\zeta) = \kappa_{\tilde{s}l} - \left(\frac{\lambda_{\tilde{s}}^2}{\alpha_l(\zeta)}\right). \tag{77}$$

In terms of the electrical engineering intensive impedance $\mathcal{Z}(\zeta)$ of the polymer DNA or RNA chain,

$$\begin{aligned} \mathcal{Z}(\zeta) &= \frac{i}{\zeta n_{\mathrm{el}} \alpha(\zeta)}, \\ \kappa(\zeta) &= \kappa_{\tilde{s}l} + i\zeta n_{\mathrm{el}} \lambda_{\tilde{s}}^2 \mathcal{Z}(\zeta), \end{aligned} \tag{78}$$

where n_{el} is the electron density per unit length of the chain. The ultrasonic attenuation of the thin molecule is determined by

$$\Im m\kappa(\omega + i0^+) = \left(n_{\mathrm{el}} \lambda_{\tilde{s}}^2\right) \omega \Re e \mathcal{Z}(\omega + i0^+) \tag{79}$$

that constitutes the mathematical expression of the physical fact that the piezoelectric coupling allows one to see in the longitudinal sound attenuation, observable by the electrical antenna impedance $\mathcal{Z}(\omega + i0^+)$.

3.5. Microbe Community Antennae

Microbial communities in the form of films adsorbed on solid substrates live much longer on insulating surfaces than on conducting metallic substances. For example, a community of COVID-19 viruses lives typically for a few days on an insulating surface but only a few hours on a metallic surface. This fact makes metallic material insertions of, for example, copper into cloth hospital face masks of some utility. Microbial communities of electrogenic bacteria adsorbed on a chemical battery cathode employ an insulating adsorption surface although the battery lead cables are eventually metallic. A working hypothesis is that the community of microbes requires, for healthy living, that DNA and RNA antennae within the community constitute a coherent phased array. The dissipative eddy currents within a metal surface will lessen the coherence of the array of antennae. Since the art of experimental biochemistry is closely entwined with the art of fine cooking, those experienced in baking bread should take note that baking yeast has DNA antennae of comparable size to bacteria. Spectroscopic measurements with a radio frequency spectrum analyzer while living processes are under way would be of interest, as would other standard Josephson array measurements long understood for superconducting arrays.

Finally, we note the possibility for large electrically connected bacterial communities (say, of millimeter or centimeter scales) of a creation of classical resonating antenna in the order of (30–300) GHz (upper end of radio wave frequencies), depending upon the exact size and shape of the community as well as nature of electrical connections within it. See also the query raised in reference [7].

4. Discussion:Some Practical Applications

All (past and present) therapeutic methods aimed at the detection or treatment of coronavirus are based on chemicals. It is tested for it (positive or negative) chemically and one hopes to cure it with a future vaccine (a chemical/genetic preparation yet to be universally tested).

If and when the virus mutates, another set of chemical protocols for its testing and a hunt for new chemicals as a vaccine shall begin: again and again. But the history of modern medicine tells us that our bio-technology is not so limited.

As discussed here, copious scientific evidence for sonic and low-energy electromagnetic signals produced by all biological elements (virus, DNA, bacteria, parasites, cells, etc.) exists; in turn, the biological elements are affected by these non-chemical signals as well. Focused research on distinct sonic and EM signals emitted by life forms can be an important non-invasive weapon in tracing unwanted life forms, and knowledge of their intensity and frequency provides important clues towards their removal. Hence, the objective of the present proposal is stated below:

Measurements and a catalog of the intensity and spectrum of these non-chemical signals (along with their careful analysis) are proposed here as a unique biophysical signature of the particular life form. Also, if and when a life form mutates, both the intensity and the frequency of the emitted signal change. Hence, such measurements would provide a dynamic real-time recording of the status of the life form. Depending upon the intensity and frequency, appropriate strategies can be defined for their removal. The relevance of the proposal for the past COVID-19 pandemic and its future avatars is obvious.

The sonic frequency of the virus (along with its intensity) can provide its *heartbeat* and act as a tracing device regarding the nature of the virus in a patient (even if judged asymptomatic through biochemical analyses). Ideally, just as the present-day pulse and the heartbeat chart (typically between 0.6 and 2 Hertz) or the brain wave chart ($\delta, \vartheta, \beta, \alpha$)-waves, spanning between 3 and 30 Hertz and slightly above for gamma- waves) inform a

clinician about the status of the general regulatory system of the patient, so can the intensity and the frequency spectrum of a virus (at much higher radio frequencies, in kilo-, mega-, or gigahertz range), provide yet another useful tool of clear benefit for the clinician and hopefully the patient.

Methodology for measurements of sonic and EM signals—discussed in the present paper—is threefold: (i) absorption of EM radiation by the life form tells us where the peak in frequency is; after which employment of resonant absorption can reduce by a factor of (2–15) the amount of radiation required for the removal of unwanted life forms to fall within safety standards; (ii) a designed digital impedance device to cross-check against data in (i) above; (iii) in vitro and in vivo animal testing models in collaboration with a company specializing in preparation of vaccines in several locations around the world.

As discussed in [7], the proposal to do resonant energy transfer from ultrasound for the destruction of the HIV virus was taken up by using efficient energy transfer from microwave radiation and mapping it out in detail against the influenza A virus [57]. The resonant peak frequency was found to be 8.2 GHz with a width of about 4 GHz. As microwave energy can be dangerous to humans and animals, it is only thanks to resonant energy transfer that the needed power was reduced by about a factor of 15 and was below the IEEE safety threshold value so that microwave power could be employed to disinfest open spaces from this virus [57]. Sun et al. [58] have studied another rod-shaped virus, WSSV (white spot syndrome virus), that is dangerous to marine life (shrimp, crab, crayfish, etc.). If we assume its mean length to be 300 nm, and the mean speed of sonar propagation as 2 km/s, its peak sonar frequency would be 6.66 GHz, which matches very well with the peak frequency of 6.5 GHz observed in Sun et al. (2017)[58]. For the internally generated EM mode frequency for this virus to be the same as the sonar frequency, we need to assume $L_{eff} = 0.78L = 234$ nm. The experimental data for this virus seem to be amenable to a satisfactory theoretical analysis using standard methods.

Oncotripsy: Selective Disruption of Cancer Cells via Resonant Ultrasound Frequency Differentiation

In a seminal paper [59], Heyden and Cortiz developed a cancer treatment procedure (called oncotripsy) that exploits differences in frequency between cancer and normal cells:

1. Frequency gaps between hepatocellular carcinoma (HCC) and healthy cells can be exploited to selectively bring the cancerous cells to lysis through the application of carefully tuned ultrasound harmonic excitation, while keeping healthy cells intact.
2. A normal mode analysis reveals the existence of a healthy-to-cancerous (HCC) spectral gap in their ground state frequency of 36.6 kHz.
3. Growth rates of the transient response of the cells to harmonic excitation reveal that lysis of cancerous cells can be achieved without damage to healthy cells.
4. Thus, oncotripsy can be a novel opportunity for cancer treatment via the application of carefully tuned ultrasound pulses in the frequency range of 80 kHz; time duration in the range of 70 microseconds and power density in the range of 0.8 W/cm^2, that is, well within the safety guidelines for the employment of ultrasound [60].
5. Such ultrasound actuation can be readily delivered by means of commercial low-frequency and low-intensity ultrasonic transducers.

Further support for oncotripsy now exists. Mittelstein et al. [61] report that unlike high-intensity ultrasound ablation of deep tissues damaging both healthy bystander tissue and cancer cells, oncotripsy with low-intensity pulsed ultrasound leverages the distinct mechanical properties of neoplastic cells to achieve inherent cancer selectivity. They show that ultrasound applied at a frequency of (0.5–0.67) MHz and a pulse duration of greater than 20 milliseconds causes selective disruption of a panel of breast, colon, and leukemia

cancer cell models in suspension without significantly damaging healthy immune or red blood cells.

The proposal to do resonant energy transfer from ultrasound for the destruction of HIV virus was made in [Babincov'a et al., 2000)][62].Subsequently, the use and mapping of efficient energy transfer from microwave radiation against the influenza A virus was done in detail by Yang et al. The resonant peak frequency was found to be 8.2 GHz with a width of about 4 GHz. As microwave energy can be dangerous to humans and animals, it is only thanks to resonant energy transfer that the needed power was reduced by about a factor of 15 and made safely below the IEEE safety threshold value so that microwave power could be employed to disinfest open spaces from this virus [57]. Also, Heyden and Ortiz posited that, by exploiting a spectral gap (of about 37 MHz) between normal and cancerous cells, cancerous cells could be selectively ablated by means of carefully tuned ultrasound while simultaneously leaving normal cells intact, an effect that they referred to as oncotripsy. Specifically, by studying the vibrational response of HCCs and healthy cells, Heyden and Ortiz found that, by carefully tuning the frequency of the harmonic excitation, lysis of the HCC nucleolus membrane could be induced selectively at no risk to healthy cells. They also estimated that the acoustic density required for oncotripsy to operate is in the low-intensity pulsed ultrasound (LIPUS) range. This low-intensity requirement sets oncotripsy apart from high-intensity focused ultrasound, which acts via thermal ablation and is non-specific, with no selectivity for cancer cells. Following these leads, Mittelstein et al. have assessed the oncotripsy effect in carefully designed laboratory tests involving a number of cancerous cell lines in aqueous suspension. They have developed a system for testing oncoptripsy that includes a tunable source of ultrasonic transduction in signal communication with a system that allows control of several parameters, including frequency and pulse duration. Transducers were selected to produce ultrasound pulses in the frequency range of approximately 100 kHz to 1 MHz, a pulse duration range of 1 ms to 1 s, acoustic intensity up to 5 Watts/cm^2 and output pressures up to 2 MPa. The instrumentation of the system allows the measurement of estimated cell death rates as a function of frequency, pressure, pulse duration, duty cycle and number of cycles. In agreement with the original oncotripsy concept, the experiments confirm that the application of LIPUS can indeed result in high death rates in the cancerous cell population selectively, i.e., simultaneously with small or zero death rates among healthy cells. The death and survival rates depend critically on the frequency of the ultrasound, indicative of a dynamical response of the cells. The oncotripsy effect is maximum at a certain frequency, and diminishes at both larger and smaller frequencies, also indicative of a resonant response of the cells. However, under the conditions of the experiments, cell death is observed to require the application of a much larger number of ultrasound cycles than anticipated, suggesting that the dynamics of cells in aqueous suspension are much more heavily damped than estimated based on the AFM measurements previously. The observations reported by Mittelstein et al. suggest that, under the conditions of the experiment, cell death occurs through a process of slow accumulation of damage over many cycles, instead of the rapid rupture of one of the cell membranes, as hypothesized earlier. It is stressed that, according to Mittelstein et al., there is very little physiological drawback arising from the oncotripsy procedure, considering that, by contrast, most chemotherapeutic medicines cause such severe damage to normal cells that often an oncologist is forced to discontinue the chemo treatment.

An exhaustive analysis of oncotripsy and various aspects of selective sonic ablation can be found in [63]. They exposed the cells in suspension for 60 s in a spatial standing wave (wavelength = 2.2 mm); a free-field pressure $P = 0.7$ MPa. The applied beam was pulsed (beam-on, beam-off with a 10% duty cycle). Very high cell-death rates were observed for both cancerous cell lines (K-562, associated with leukemia and U-937, associated with

pleura/pleural effusion, lymphocyte, myeloid) at an applied frequency of 500 kHz and a 20-millisecond duration. By contrast, under identical conditions, the control (healthy CD4 T-cells) remained nearly unaffected. Their observations bear out the efficacy of oncotripsy as a frequency-dependent resonant response leading to eventual death of selectively targeted cells.

Below we summarize some of their other important findings regarding cyto-disruption, death and repair rates for cells when under insonation.

1. The behavior of cells depends crucially upon their surrounding environment matrix (aqueous versus extracellular matrix, ECM considered in ref. ([59]) for instance).
2. Oncotripsy becomes more and more effective as the damping frequency gets closer and closer to the natural frequency of the cell.

Thus, resonant frequency ultrasound beamed to a cancer patient shows that cancerous cells are indeed depleted by such a technique [64]. Clearly, further work is required to streamline and perfect this promising technique.

5. Conclusions

Electrogenic micro-organisms live within environments wherein they are wired to one another or are wired to the environmental surfaces. Electronic currents can flow through these wires into and out of biological cells through the cell walls. Of interest in the work described above was the wireless communication that can be radiated from a distance into and out of biological cells wherein the DNA or the RNA molecules can act as antennae that receive or emit radio frequency electromagnetic signals. As an alternative to the chemical information carried in the DNA or RNA letter coding, communication information can be carried from a distance in the form of thermodynamic radiation signal entropy. Due to biological piezoelectricity, the electromagnetic radiation is appreciably coupled into ultrasonic acoustic radiation. Thus, electromagnetic as well as acoustic spectroscopy is evidently possible.

The helices or double helices, respectively, within RNA and DNA exhibit chiral symmetry breaking (handedness), as must the electronic energy structure. The electronic structure must also properly require chiral symmetry breaking. The electron as an elementary particle carries two possible spin states $\uparrow$ or $\downarrow$ as well as two chiral states right R or left L. Thus, we argued, as discovered by Dirac, the electron requires a four-component spinor for its description. These four components are required for describing chiral symmetry breaking even if the electrons have kinetic energies small on the scale of the electron rest mass energy.

DNA and RNA as long polymer molecules are quasi one-dimensional. This, coupled with the chiral symmetry breaking, suggested that the electronic structure has the structure of a Tomonaga–Luttinger liquid wherein the particle-hole bound states. The bound state of an electron particle-hole pair is a boson, and the Tomonaga–Luttinger liquid is condensation of these bosons in a manner closely analogous to the Bose condensation of particle-particle or hole-hole bound states in a superconductor. In a superconductor, the phase of the Bose pairing field gives rise to Josephson effects. In the biological Tomonaga–Luttinger electron liquid, we employed the phase difference between right- and left-handed electron components to describe the quantum coherence leading to Josephson effects. In both cases, the Josephson effects lead to a quantum pendulum, i.e., a sine-Gordon boson field model as first demonstrated by Coleman. The physical principle involved is that Josephson effects occur whenever the coherent quantum liquid is forced to flow through weak links; quantum pendulum dynamics holds sway.

We have begun what we hope will be the beginning of the study of wireless electrodynamic communication between biological cells starting with (say) bacteria or viruses that

have DNA or RNA within the cell nucleus. The basic DNA and RNA microbe antennae must be wired in nature as a biological community of coherent phased antenna arrays for appreciable communication information bit-rates radiated through large distances. Arrays of biological weak links might serve that purpose.

Author Contributions: Conceptualization, A.W. and M.N.; Methodology, J.S. and M.N.; Software, G.d.M., D.D. and E.S.; Formal analysis, E.S.; Investigation, J.S.; Data curation, D.D.; Writing – original draft, A.W. and Y.S.; Writing – review & editing, Y.S., D.D. and E.S.; Supervision, Y.S.; Project administration, Y.S. and G.d.M. All authors have read and agreed to the published version of the manuscript.

Funding: This research received no external funding.

Institutional Review Board Statement: Not applicable.

Informed Consent Statement: Not applicable.

Data Availability Statement: No new data were created or analyzed in this study. Data sharing is not applicable to this article.

Conflicts of Interest: The authors declare no conflicts of interest.

Appendix A. Capacitance and Inductance per Unit Length

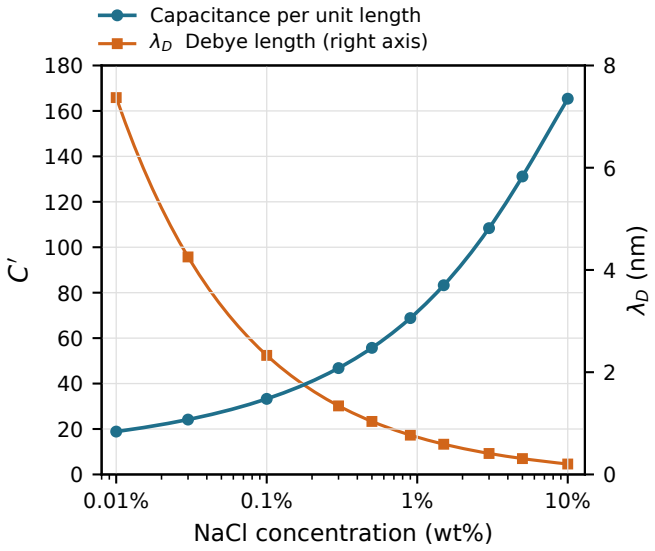

Figure A1. Shown is the capacitance per unit length for a DNA helix modeled as a cylinder with an inner radius $a = 1$ nm surrounded by a counter-ion Debye sheath. It depends upon the solution's dielectric constant.

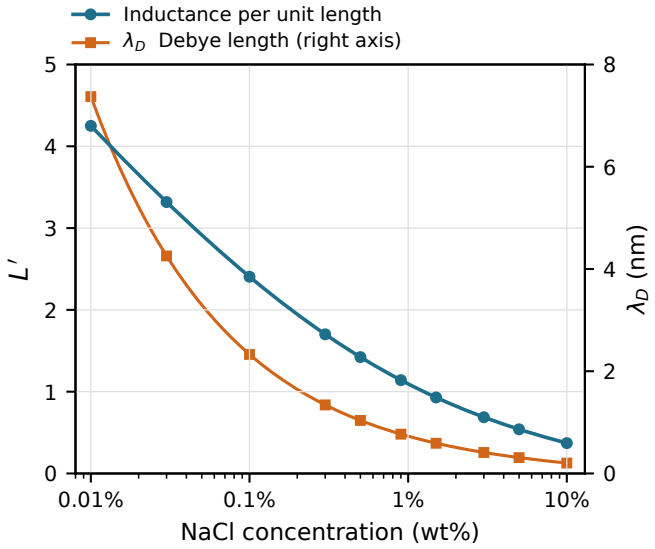

Figure A2. Shown is the inductance per unit length for a DNA helix modeled as a cylinder with an inner radius $a = 1$ nm surrounded by a counter-ion Debye sheath. It does not depend on the solution's dielectric constant.

Consider a DNA helix as a cylinder with inner radius $a = 1$ nm surrounded by a counter-ion Debye sheath of length λ_D so that the outer radius becomes $b = a + \lambda_D$. Then, one may consider the capacitance per unit length (ϵ) and inductance per unit length (μ) as modeled by a coaxial line as follows:

$$\begin{aligned}
\epsilon &= \frac{\epsilon_r(M)}{2\ln(b/a)}; (i); \\
\mu &= \frac{2}{c^2}\ln(b/a); (ii); \\
\text{Debye length } \lambda_D &= \frac{0.304}{\sqrt{c}} nm; (iii); \\
\text{molarity} M &= 0.171 \times (wt\%) mol/L; (iv); \\
\epsilon_r(M) &\approx 80.1 - 8.0M; (v);
\end{aligned} \tag{A1}$$

Unlike the inductance, the capacitance per unit length depends upon the solution's dielectric constant ($\epsilon_r(M)$) [vedi Equation (A1)(i),(v)] [65].

References

1. Tsvelik, A. *Quantum Field Theory in Condensed Matter Physics*, 2nd ed.; Cambridge University Press: Cambridge, UK, 2003.
2. Giudice, E.D.; Doglia, S.; Milani, M.; Vitiello, G. A quantum field theoretical approach to the collective behaviour of biological systems. *Nucl. Phys.* **1985**, *251*, 375–400.
3. Abrikosov, A.A.; Gorkov, I.P.; Dzyaloshinski, I.E. *Methods of Quantum Field Theory in Statistical Physics*; Dover Publications: New York, NY, USA, 1968.
4. Percus, J.K. *Mathematics of Genome Analysis*; Cambridge University Press: Cambridge, UK, 2001.
5. Landau, L.D.; Lifshitz, E.M. *Electrodynamics of Continuous Media*; Pergamon Press: Oxford, UK, 1984.
6. Manton, N.; Sutcliffe, P. *Topological Solitons*; Cambridge University Press: Cambridge, UK, 2004.
7. Srivastava, Y.N.; Swain, J.; Widom, A.; Narain, M.; de Montmollin, G.; Sassaroli, E. Non-chemical signatures of biological materials: Radio signals from Covid19? *Electromagn. Biol. Med.* **2020**, *39*, 340–346.
8. Widom, A.; Swain, J.; Srivastava, Y.N.; Sivasubramanian, S. Electromagnetic Signals from Bacterial DNA. *arXiv* **2012**, arXiv:1104.3113v2.
9. Swain, J.; Srivastava, Y.; Widom, A. Wireless electromagnetic communication systems between bacteria in communities. *Key Eng. Mater.* **2013**, *543*, 318–321.

10. Widom, A.; Srivastava, Y.; Valenzi, V. The Biophysical Basis of Benveniste Experiments: Entropy, Structure, and Information in Water. *Int. J. Quantum Chem.* **2010**, *110*, 252–256.
11. Teskea, A. Cable Bacteria: Living Electrical Conduits in the Microbial World. *Proc. Natl. Acad. Sci. USA* **2019**, *116*, 18759–18761.
12. Reguera, G. Biological Electron Transport goes the Extra Mile. *Proc. Natl. Acad. Sci. USA* **2018**, *115*, 5632–5634.
13. Kiseleva, L.; Briliute, J.; Khilyas, I.V.; Simpson, D.J.W.; Fedorovich, V.; Cohen, M.; Goryanin, I. Magnet-Facilitated Selection of Electrogenic Bacteria from Marine Sediment. *BioMed Res. Int.* **2015**, *2015*, 582471.
14. Gorby, Y.A.; Yanina, S.; McLean, J.S.; Rosso, K.M.; Moyles, D.; Dohnalkova, A.; Beveridge, T.J.; Chang, I.S.; Kim, B.H.; Kim, K.S.; et al. Electrically Conductive Bacterial Nanowires Produced by Shewanella Oneidensis Strain MR-1 and other Microorganisms. *Proc. Natl. Acad. Sci. USA* **2006**, *103*, 11358–11363. Correction in *Proc. Natl. Acad. Sci. USA* **2009**, *106*, 9535.
15. Naureen, Z.; Al Matani, Z.A.R.; Al Jabri, M.N.; Al Housni, S.K.; Gilani, S.A.; Mabood, F.; Farooq, S.; Hussain, J.; Al Harrasi, A. Generation of Electricity by Electrogenic Bacteria in a Microbial Fuel Cell Powered by Waste Water. *Adv. Biosci. Biotechnol.* **2016**, *7*, 329–335.
16. Ntarlagiannis, D.; Atekwana, E.A.; Hill, E.A.; Gorby, Y. Microbial nanowires: Is the subsurface "hardwired"? *Geophys. Res. Lett.* **2007**, *34*, L17305.
17. Crick, F. On Protein Synthesis, The Biological Replication of Macromolecules. *Symp. Soc. Exp. Biol.* **1958**, *12*, 138–163.
18. Sarkar, S. *Biological Information: A Skeptical Look at Some Central Dogmas of Molecular Biology*, *The Philosophy and History of Molecular Biology: New Perspectives*; Sarkar, S., Ed.; Kluwer Academic: Dordrecht, The Netherlands; Boston, MA, USA, 1996; pp. 187–232.
19. Smith, J.M. The Concept of Information in Biology. *Philos. Sci.* **2000**, *67*, 177–194.
20. Artiga, M. Biological Information. In *The Stanford Encyclopedia of Philosophy*, 2024 ed.; Zalta, E.N., Nodelman, U., Eds.; Available online: https://plato.stanford.edu/archives/sum2025/entries/information-biological/ (accessed on).
21. Shannon, C.E. A Mathematical Theory of Communication. *Bell Syst. Tech. J.* **1948**, *27*, 379–423.
22. Adami, C. Use of Information Theory in Evolutionary Biology. *Ann. N. Y. Acad. Sci.* **2012**, *1256*, 49–65.
23. Koonin, E.V. The meaning of biological information. *Philos. Trans. R. Soc. A Math. Phys. Eng. Sci.* **2016**, *374*, 20150065.
24. Kuruoglu, E.E.; Arndt, P.F. The information capacity of the genetic code: Is the natural code optimal? *J. Theor. Biol.* **2017**, *419*, 227–237.
25. Dickins, C. The role of information in evolutionary biology. *Acta Biotheor.* **2023**, *71*, 17.
26. Sherwin, W. Pan-Evo: The evolution of information and Biology's part in this. *Biology* **2024**, *13*, 507.
27. Wagner, A. Information theory, evolutionary innovations and evolvability. *Phil. Trans. Royal Soc. B* **2017**, *352*, 20160416.
28. Dicke, R. Coherence in Spontaneous Radiation Processes. *Phys. Rev.* **1954**, *93*, 99–110.
29. Hepp, K.; Lieb, E. Equilibrium Statistical Mechanics of Matter Interacting with the Quantized Radiation Field. *Phys. Rev. A* **1973**, *8*, 2517–2525.
30. Giudice, E.D.; Preparata, G.; Vitiello, G. Water as a Free Electric Dipole Laser. *Phys. Rev. Lett.* **1988**, *61*, 1085.
31. Sivasubramanian, S.; Srivastava, Y.; Widom, A. Landau Ghosts and Anti-Ghosts in CondensedMatter and High Density Hadronic Matter. *Mod. Phys. Lett.* **2002**, *B16*, 1201–1209.
32. Robinson, R.; Stokes, R. *Electrolyte Solutions*; Dover Publications Inc.: New York, NY, USA, 1959.
33. Frank, H.; Evans, M. Free Volume and Entropy in Condensed Systems III. Entropy in Binary Liquid Mixtures; Partial Molal Entropy in Dilute Solutions; Structure and Thermodynamics in Aqueous Electrolytes. *J. Chem. Phys.* **1945**, *13*, 507–532.
34. Montagnier, L.; Aïssa, J.; Ferris, S.; Montagnier, J.L.; Lavallee, C. Electromagnetic signals are produced by aqueous nanostructures derived from bacterial DNA sequences. *Interdiscipl. Sci. Comput. Life Sci.* **2009**, *1*, 81–90.
35. Rao, M.; Sarabandi, K.; Soukar, J.; Kotov, N.; VanEpps, J. Experimental Evidence of Radio Frequency Radiation From Staphylococcus aureus Biofilms. *IEEE J. Electromagn. Microwaves Med. Biol.* **2022**, *6*, 420–428.
36. Barani, N.; Sarabandi, K.; Kotov, N.; Vanepps, J.; Elvati, P.; Wang, Y.; Violi, A. A Multiphysics Modeling of Electromagnetic Signaling Phenomena at KHz-GHz Frequencies in Bacterial Biofilms. *IEEE Access* **2022**, *10*, 39344–39361.
37. Telega, J.J.; Wojenar, R. Piezoelectric Effects in Biological Tissues. *J. Theor. Appl. Mech.* **2002**, *40*, 3.
38. Shamos, M.; Lavine, L. Piezoelectricity as a Fundamental Property of Biological Tissues. *Nature* **1967**, *213*, 267–269.
39. Tomonaga, S. Remarks on Block's Method of Sound Waves Applied to Many Fermion Problems. *Prog. Theor. Phys.* **1950**, *5*, 544–569.
40. Luttinger, J.M. An Exactly Soluble Model of a Many Fermion System. *J. Math. Phys.* **1963**, *4*, 1154–1162.
41. Mattis, D.C.; Lieb, E.H. Exact Solution of a Many Fermion System and Its Associated boson Field. *J. Math. Phys.* **1963**, *6*, 304–312.
42. Preparata, G. *QED Coherence in Matter*; World Scientific Publications: Singapore, 1995.
43. Coleman, S. Quantum sine-Gordon equation as the massive Thirring model. *Phys. Rev. D* **1975**, *11*, 2088–2097.
44. Su, W.P.; Schrieffer, J.R.; Heeger, A.J. Solitons in Polyacetylene. *Phys. Rev. Lett.* **1979**, *42*, 1698.
45. Heeger, A.J.; Kivalson, S.; Schrieffer, J.R.; Su, W.P. Solitons in Conducting Polymers. *Rev. Mod. Phys.* **1988**, *60*, 781.
46. Jackiw, R.; Rebbi, C. Solitons with Fermion Number 1/2. *Phys. Rev. D* **1976**, *13*, 3398–3409.

47. Meier, E.; An, F.; Gadway, B. Observation of the Topological Soliton State in the Su Schrieffer Heeger Model. *Nat. Commun.* **2016**, *7*, 13986.
48. Marantan, A.; Mahadevana, L. Mechanics and Statistics of the Worm-Like Chain. *Am. J. Phys.* **2018**, *86*, 86–94.
49. Ogden, R.W.; Saccomandi, G.; Sgura, I. On Wormlike Chain Models within the Three-Dimensional Continuum Mechanics Framework. *Proc. Roy. Soc. A* **2006**, *462*, 749–768.
50. Kühnel, W. *Differential Geometry: Curves, Surfaces, Manifolds*; AMS: Providence, RI, USA, 2005.
51. Doi, M.; Edwards, S.F. *The Theory of Polymer Dynamics*; Oxford University Press: Oxford, UK, 1988.
52. Li, X.; Schroeder, M.C.; Dorman, K.D. Modeling the Stretching of Wormlike Chains in the Presence of Excluded Volume. *Soft Matter* **2015**, *11*, 5947–5954.
53. Landau, L.D.; Lifshitz, E.M. *Theory of Elasticity*; Pergamon Press: Oxford, UK, 1970.
54. Guidice, E.D.; Preparata, G. Proceedings International Conference on Macroscopic Quantum Coherence. In *A New QED Picture of Water: Understanding a Few Fascinating Phenomena*; Sassaroli, E., Srivastava, Y., Swain, J., Widom, A., Eds.; World Scientific: Singapore, 1997.
55. Bhatia, A.B. *Ultrasonic Absorbtion*; Oxford University Press: Oxford, UK, 1967.
56. Diethelm, K. *The Analysis of Fractional Differential Equations: An Application-Oriented Exposition Using Differential Operators of Caputo*; Springer: Berlin/Heidelberg, Germany, 2010.
57. Yang, S.; Lin, H.C.; Liu, T.M.; Lu, J.T.; Hung, W.T.; Huang, Y.R.; Tsai, Y.C.; Kao, C.L.; Chen, S.Y.; Sun, C.K. Efficient structure resonance energy transfer from microwaves to confined acoustic vibrations in viruses. *Nat. Sci. Rep.* **2015**, *5*, 18030.
58. Sun, C.; Tsai, Y.C.; Chen, Y.J.E.; Liu, T.M.; Chen, H.Y.; Wang, H.C.; Lo, C.F. Resonant dipolar coupling of microwaves with confined acoustic vibrations in a rod-shaped virus. *Nat. Sci. Rep.* **2017**, *7*, 4611.
59. Heyden, S.; Ortiz, M. Oncotripsy: Targeting cancer cells selectively via resonant harmonic excitation. *J. Mech. Phys. Solids* **2016**, *92*, 164–175. *Comput. Methods Appl. Mech. Eng.* **2017**, *314*, 314.
60. *SCC39*; IEEE Standard for Safety Levels with Respect to Human Exposure to Radio Frequency Electromagnetic Fields, 3 kHz to 300 GHz. IEEE International Committee on Electromagnetic Safety: New York, NY, USA, 19 April 2006.
61. Mittelstein, D.; Ye, J.; Schibber, E.F.; Roychoudhury, A.; Martinez, L.T.; Fekrazad, M.H.; Ortiz, M.; Lee, P.P.; Shapiro, M.G.; Gharib, M. Selective ablation of cancer cells with low intensity pulsed ultrasound. *Appl. Phys. Lett.* **2019**, *116*, 013701.
62. Babincová, M.; Sourivong, P.; Babinec, P. Resonant absorption of ultrasound energy as a method of HIV destruction. *Medical Hypotheses* **2000**, *55*, 450-451.
63. Schibber, E.; Mittelstein, D.R.; Gharib, M.; Shapiro, M.G.; Lee, P.P.; Ortiz, M. A dynamical model of oncotripsy by mechanical cell fatigue: Selective cancer cell ablation by low-intensity pulsed ultrasound. *Proc. R. Soc. A* **2020**, *476*, 20190692.
64. Heyden, S.; Ortiz, M. Oncotripsy: Targeting cancer cells selectively via resonant harmonic excitation. *arXiv* **2020**, arXiv:1512.03320v2.
65. Hasted, J.; Ritson, D.; Collie, C. Dielectic properties of aqueous ionic solutions. Parts I and II. *J. Chem. Phys.* **1948**, *16*, 1–21.

Disclaimer/Publisher's Note: The statements, opinions and data contained in all publications are solely those of the individual author(s) and contributor(s) and not of MDPI and/or the editor(s). MDPI and/or the editor(s) disclaim responsibility for any injury to people or property resulting from any ideas, methods, instructions or products referred to in the content.